Integrated Guidance, Navigation, and Control System for a UAV in a GPS Denied Environment

Ju-Hyeon Hong[1], Chang-Kyung Ryoo[2], Hyo-Sang Shin[1] and Antonios Tsourdos[1]

[1]*School of Aerospace, Transportation, and Manufacturing, Cranfield University, College Road, MK43 0AL, Cranfield, U.K.*
[2]*Aerospace Engineering, Inha University, 100 Inharo, Namgu, 22212, Incheon, Republic of Korea*

Keywords: GPS Denied Environment, Indoor Flight, Integrated Guidance Navigation and Control System, Visual Guidance and Control.

Abstract: This paper proposes an integrated guidance, navigation, and control system for operations of a UAV in GPS denied environments. The proposed system uses a sensor combination, which consists of an image sensor and a range sensor. The main idea of the system developed is that it replaces the conventional navigation information with the measurement from the image processing. For example, it is possible to substitute the look angle and look angle rate from the image sensor for the conventional navigation information like the relative target position and the body angular rate. As the preliminary study, the integrated guidance and control system is designed with a nonlinear back-stepping approach to investigate the possibility of the proposed system. And the proposed integrated guidance and control system is verified by the numerical simulation.

1 INTRODUCTION

The large scale of small Unmanned Aerial Vehicle (UAV) applications has proliferated vastly within the last few years. The operational experience of UAVs has proven that their technology can bring a dramatic impact to military and civilian areas. There are numerous potential applications under consideration and being studied at the moment.

One of interesting aspects in applications of small UAVs is that they might need to be operated in a GPS denied environment such as inside a building. In such a case, the most common navigation system in aerospace, namely INS/GPS system is not applicable and hence other means of navigation should be sought for.

Simultaneous localization and mapping (SLAM) and the visual odometry are two common alternative navigation systems that could be implemented in a GPS denied environment or indoor environment. (Achtelik et al., 2009; Ahrens et al., 2009; Alarcon et al., 2015; Blösch et al., 2010; Çelik and Somani, 2009; Chowdhary et al., 2013; Ghadiok et al., 2011; Kendoul et al., 2009) Although they can provide reasonable performance, they might be subject to a relatively complex sensor combination or require

high computational power. Since the operations of small UAVs are constrained by limited payload and power, applying the two systems might become restricted in practice.

Under these backgrounds, this paper aims to develop a new navigation system that is suitable for operations of a small UAV in a GPS denied environment. The focus of the development is to test how far we can push in terms of the types and number of sensors required. The guidance, navigation and control (GNC) systems are the main driver determining sensor requirements. Therefore, this study also focuses to come up with an appropriate GNC system for the sensor combination selected.

The sensor combination proposed and tested in this paper consists of only an image sensor and a range sensor. We intend to investigate whether it is possible to abandon the need for an inertial measurement unit (IMU), which plays the most crucial role in navigation, up to the best of our knowledge. Note that the proposed sensor combination cannot provide all information required for the conventional GNC systems. Therefore, this paper also develops an integrated guidance and control (IGC) system that requires the navigation information obtainable from the proposed sensor

combination. The feasibility of the proposed approach is investigated through initial theoretical analysis and numerical simulations.

The rest of this paper is organised as follows. In section 2, the mathematical models for UAV dynamics and relative navigation information are presented. Section 3 introduces the structure of the integrated guidance, navigation, and control system, which is a key contribution of this paper. To verify the proposed integrated guidance and control system, the results of the numerical simulation are presented in section 4. Conclusion of this paper is given in section 5.

2 PROBLEM DEFINITION

2.1 6-DOF Dynamics of the UAV

To design the guidance and control system, 6-DOF dynamics are formulated. The mathematical models are based on following assumptions.

- The body and propeller of a quadcopter are rigid and symmetric.
- The thrust force is proportional to the square of motor's speed.
- The earth rotation can be ignored.
- The inertial coordinate system is a flat earth model.

The coordinate system and forces for the UAV model are shown in Figure 1. The inertial frame is a north-east-down frame (n-frame). And the body frame (b-frame) is a fixed frame of the body of the UAV.

Let $\begin{bmatrix} r_x^n & r_y^n & r_z^n \end{bmatrix}^T$ and $\begin{bmatrix} \phi & \theta & \psi \end{bmatrix}^T$ denote a position vector in n-frame and an attitude angle vector respectively. The aerodynamic friction coefficients are K_t and K_r respectively. The mass and vector of the moment of inertia are m and $\begin{bmatrix} I_{xx}, I_{yy}, I_{zz} \end{bmatrix}$ respectively. The thrust force and vector of the moment are respectively T and $\begin{bmatrix} M_x & M_y & M_z \end{bmatrix}^T$. The vector of body angular rate is $\begin{bmatrix} p & q & r \end{bmatrix}^T$. The dynamic model of the UAV is given as follows:

$$\begin{bmatrix} \ddot{r}_x^n \\ \ddot{r}_y^n \\ \ddot{r}_z^n \end{bmatrix} = \begin{bmatrix} 0 \\ 0 \\ g \end{bmatrix} - \frac{T}{m} \begin{bmatrix} c\theta c\psi \\ s\phi s\theta c\psi - c\phi s\psi \\ c\phi s\theta c\psi + s\phi s\psi \end{bmatrix} + \frac{K_t}{m} \begin{bmatrix} \dot{r}_x^n \\ \dot{r}_y^n \\ \dot{r}_z^n \end{bmatrix} \quad (1)$$
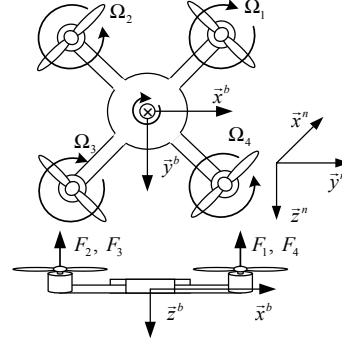

Figure 1: The coordinate system for a quadcopter.

$$\begin{bmatrix} \ddot{\phi} \\ \ddot{\theta} \\ \ddot{\psi} \end{bmatrix} = \begin{bmatrix} 1 & t\theta s\phi & t\theta c\phi \\ 0 & c\phi & -s\phi \\ 0 & s\phi sc\theta & c\phi sc\theta \end{bmatrix} \begin{bmatrix} \dot{p} \\ \dot{q} \\ \dot{r} \end{bmatrix} + \dot{R}_r \begin{bmatrix} p \\ q \\ r \end{bmatrix} \quad (2)$$

where

$$\dot{R}_r = \begin{bmatrix} 0 & s\phi/c^2\theta\dot{\theta} & c\phi/c^2\theta\dot{\theta} \\ & +t\theta c\phi\dot{\phi} & -t\theta s\phi\dot{\phi} \\ 0 & -s\phi\dot{\phi} & -c\phi\dot{\phi} \\ 0 & t\theta s\phi/c\theta\dot{\theta} & t\theta c\phi/c\theta\dot{\theta} \\ & +c\phi/c\theta\dot{\phi} & -s\phi/c\theta\dot{\phi} \end{bmatrix} \quad (3)$$

$$\begin{bmatrix} \dot{p} \\ \dot{q} \\ \dot{r} \end{bmatrix} = \begin{bmatrix} \dfrac{I_{yy} - I_{zz}}{I_{xx}} qr \\ \dfrac{I_{zz} - I_{xx}}{I_{yy}} pr \\ \dfrac{I_{xx} - I_{yy}}{I_{zz}} qr \end{bmatrix} + \begin{bmatrix} 0 \\ 0 \\ g \end{bmatrix} + \begin{bmatrix} M_x/I_{xx} \\ M_y/I_{yy} \\ M_z/I_{zz} \end{bmatrix} - \frac{K_r}{m} \begin{bmatrix} p \\ q \\ r \end{bmatrix} \quad (4)$$

The forces of motors are given by :

$$F_i = k\Omega_i^2, \ (i = 1, 2, 3, \ and, \ 4) \quad (5)$$

where k and Ω_i are the motor parameter and the rotational speed of the i-th motor. The thrust force and moment can be expressed by the forces of the motors:

$$\begin{bmatrix} T \\ M_x \\ M_y \\ M_z \end{bmatrix} = \begin{bmatrix} 1 & 1 & 1 & 1 \\ l & l & -l & -l \\ l & -l & -l & l \\ c & c & c & c \end{bmatrix} \begin{bmatrix} F_1 \\ F_2 \\ F_3 \\ F_4 \end{bmatrix} \quad (6)$$

where l and c are the distance of the moment arm and the drag factor.

2.2 Relative Navigation Information from Camera Frame

This section introduces the process for relative navigation information in the camera frame (c-frame). The relative navigation information can be expressed by a target vector from UAV to the target in the c-frame. Figure 2 shows the target vector in c-frame. The focal length of the camera and the look angle vector are f and $\left[\lambda_\theta, \lambda_\psi\right]$ respectively. The unit target vector in c-frame is given as:

$$\vec{u}^c = \frac{\cos\lambda_\psi \cos\lambda_\theta}{f}\begin{bmatrix} f \\ f\tan\lambda_\psi \\ -f\tan\lambda_\theta\sec\lambda_\psi \end{bmatrix} = \begin{bmatrix} c\lambda_\psi c\lambda_\theta \\ s\lambda_\psi c\lambda_\theta \\ -s\lambda_\theta \end{bmatrix} \quad (7)$$

The unit target vector in the b-frame can be expressed as the unit vector in the look angle frame (λ -frame).

$$\vec{u}^b = \begin{bmatrix} c\lambda_\psi & s\lambda_\psi & 0 \\ -s\lambda_\psi & c\lambda_\psi & 0 \\ 0 & 0 & 1 \end{bmatrix}^T \begin{bmatrix} c\lambda_\theta & 0 & -s\lambda_\theta \\ 0 & 1 & 0 \\ s\lambda_\theta & 0 & c\lambda_\theta \end{bmatrix}^T \begin{bmatrix} 1 \\ 0 \\ 0 \end{bmatrix}$$
$$= \begin{bmatrix} c\lambda_\theta c\lambda_\psi \\ c\lambda_\theta s\lambda_\psi \\ -s\lambda_\theta \end{bmatrix} \quad (8)$$

The unit target vector in c-frame and the unit target vector in b-frame are the same. Therefore the look angle can be obtained by the target vector in c-frame.

$$\lambda_\psi = \tan^{-1}\left(\frac{r_y^c}{f}\right), \quad \lambda_\theta = \tan^{-1}\left(\frac{-r_z^c}{\sqrt{f^2 + \left(r_y^c\right)^2}}\right) \quad (9)$$

The main idea of the proposed the GNC system is based on the physical characteristic of the look angle.
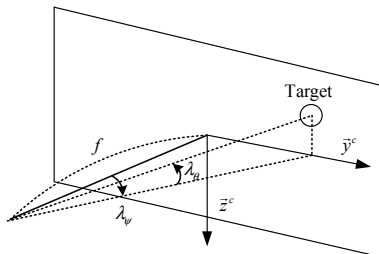

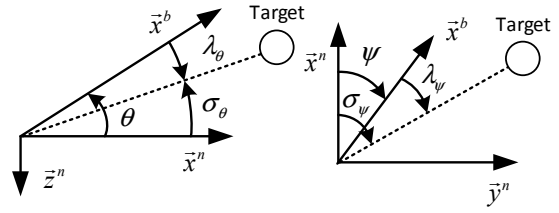Figure 2: The target information in camera frame.

Figure 3: Definition of the LOS angle and look angle.

Let us define the LOS angle to investigate the characteristic of the look angle. The relationship between the LOS angle, the look angle, and the attitude angle is shown in

Figure 3. Let define LOS angles $\left[\sigma_\theta, \sigma_\psi\right]$ to describe the target vector in the n-frame.

$$\sigma_\psi = \tan^{-1}\left(\frac{r_y^n}{r_x^n}\right), \quad \sigma_\theta = \tan^{-1}\left(\frac{r_z^n}{\sqrt{\left(r_x^n\right)^2 + \left(r_y^n\right)^2}}\right) \quad (10)$$

From the LOS angle, the target vector in the n-frame can be calculated directly. However, by using the fixed image sensor, the UAV can obtain the target vector in the b-frame. It means that the look angle describes not only the variation of the target relative position, but also the variation of the attitude angle. If the pitch and yaw plane can be decoupled by stabilizing roll axis, the look angle can be defined as follows:

$$\begin{aligned} \lambda_\theta &= \sigma_\theta - \theta \\ \lambda_\psi &= \sigma_\psi - \psi \end{aligned} \quad (11)$$

When the UAV moves slowly, the attitude angles of the UAV are small. It means that the look angles are nearly the same as the LOS angles. Therefore the look angle can replace the LOS angle at slow speed. Moreover the look angle rate can be described by the derivative of eq.(11):

$$\begin{aligned} \dot{\lambda}_\theta &= \dot{\sigma}_\theta - \dot{\theta} \\ \dot{\lambda}_\psi &= \dot{\sigma}_\psi - \dot{\psi} \end{aligned} \quad (12)$$

As shown in eq.(12), the look angle rates include the LOS rate and the attitude angle rate. For this reason, if the look angle rates are stabilised to zero, the body angular rates are also conversed to zero. By theses physical characteristics of the look angle, the look angles and the look angle rates can be replaced with the LOS angle and the body angular rate respectively. In the next section, the GNC system, which is based on these characteristic, is introduced.

3 INTEGRATED GUIDANCE, NAVIGATION AND CONTROL (IGNC) SYSTEM

The general system framework of the conventional guidance and control is shown in Figure 4. Normally, the guidance and navigation system utilizes four types of sensors, i.e., a gyroscope, an accelerometer, a magnetometer, and a GPS. On the other hand, this paper proposes to use an image sensor and a range meter for our proposed guidance and navigation system to allow operation of such system in a GPS-denied environment. The structure of the proposed guidance and control system is shown in Figure 5. The proposed guidance and control system utilizes the relative information measured by the image sensor and the range meter. The navigation filter, then provides the information required for the new guidance and navigation.

The detailed structure of the IGNC system is given in Figure 6. The target vector in c-frame and the relative distance are measured by the image sensor and the range sensor in the target tracking system. In addition, the target images are used for estimating the attitude angles by the image processing algorithm. The outputs of the target tracking system are used for the measurement of the relative navigation filter. Moreover the outputs of the relative navigation filter are used in the proposed integrated guidance and control (IGC) system. Finally the IGC system calculates the thrusts of the UAV.
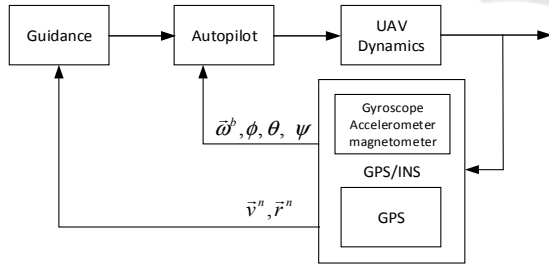

Figure 4: The conventional guidance and control system.
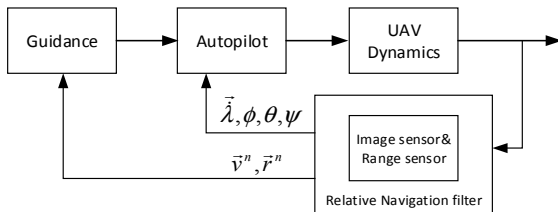

Figure 5: The proposed guidance navigation and control system.
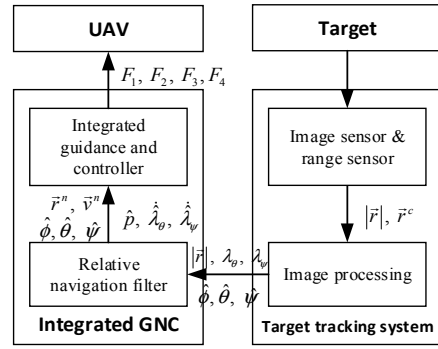

Figure 6: Integrated control and guidance system.

Since the scope of this paper is to confirm the possibility of the IGC system, the relative navigation filter is regarded as the ideal model in the numerical simulation. In following sub-sections, the structures of the relative navigation filter and the IGC system are presented.

3.1 Relative Navigation Filter

The relative navigation filter estimates the relative velocity, the look angle rate and the roll rate. The relative position can be expressed as:

$$\vec{r}^n = C_b^n \, |\vec{r}| \begin{bmatrix} c\,\lambda_\theta\,c\,\lambda_\psi & c\,\lambda_\theta\,s\,\lambda_\psi & -s\,\lambda_\theta \end{bmatrix}^T \quad (13)$$

where C_b^n is a coordinate transformation matrix from the b-frame to the n-frame. Since the relative velocity, the roll rate and the look angle rate are the derivatives of the relative position, the roll angle, and the look angle, these parameters can be estimated by the simple alpha-beta filter. Therefore the state vector of the relative navigation filter is given as

$$X = \begin{bmatrix} \lambda & \dot{\lambda} & r_x^n & v_x^n & r_y^n & v_y^n & r_z^n & v_z^n & \phi & p \end{bmatrix}^T$$

and the measurement vector of the relative navigation filter is given as $Z = \begin{bmatrix} \lambda & r_x^n & r_y^n & r_z^n & \phi \end{bmatrix}^T$. The propagation model and update model of the relative navigation filter can be expressed as:

$$\bar{X}(k) = \hat{X}(k-1) + F\hat{X}(k-1) \quad (14)$$

$$\hat{X}(k) = \bar{X}(k) + K\big(Z(k) - H\bar{X}(k)\big) \quad (15)$$

where K is the filter gain matrix. The system matrix F and the measurement matrix H are given as :

$$F = \begin{bmatrix} 1 & dt & 0 & 0 & 0 & 0 & 0 & 0 & 0 & 0 \\ 0 & 1 & 0 & 0 & 0 & 0 & 0 & 0 & 0 & 0 \\ 0 & 0 & 1 & dt & 0 & 0 & 0 & 0 & 0 & 0 \\ 0 & 0 & 0 & 1 & 0 & 0 & 0 & 0 & 0 & 0 \\ 0 & 0 & 0 & 0 & 1 & dt & 0 & 0 & 0 & 0 \\ 0 & 0 & 0 & 0 & 0 & 1 & 0 & 0 & 0 & 0 \\ 0 & 0 & 0 & 0 & 0 & 0 & 1 & dt & 0 & 0 \\ 0 & 0 & 0 & 0 & 0 & 0 & 0 & 1 & 0 & 0 \\ 0 & 0 & 0 & 0 & 0 & 0 & 0 & 0 & 1 & dt \\ 0 & 0 & 0 & 0 & 0 & 0 & 0 & 0 & 0 & 1 \end{bmatrix} \qquad (16)$$

$$H = \begin{bmatrix} 1 & 0 & 0 & 0 & 0 & 0 & 0 & 0 & 0 & 0 \\ 0 & 0 & 1 & 0 & 0 & 0 & 0 & 0 & 0 & 0 \\ 0 & 0 & 0 & 0 & 1 & 0 & 0 & 0 & 0 & 0 \\ 0 & 0 & 0 & 0 & 0 & 0 & 1 & 0 & 0 & 0 \\ 0 & 0 & 0 & 0 & 0 & 0 & 0 & 0 & 1 & 0 \end{bmatrix} \qquad (17)$$

where dt is the time step.

3.2 Integrated Guidance and Control (IGC) System

As the dynamics of the UAV are nonlinear, a nonlinear back-steeping approach is applied for IGC. Note that the back-stepping approach designed in this paper is based on the method developed in (Madani and Benallegue, 2006). The control input vector is the derivatives of the thrusts of the four motors and it is given as $u = \begin{bmatrix} \dot{F}_1 & \dot{F}_2 & \dot{F}_3 & \dot{F}_4 \end{bmatrix}^T$.

The dynamic equations are expressed in the state-space form as follows:

$$\begin{aligned}
\dot{x}_1 &= \begin{bmatrix} v_x^n & v_y^n \end{bmatrix}^T \\
\dot{x}_2 &= \begin{bmatrix} \dot{v}_x^n & \dot{v}_y^n \end{bmatrix}^T \\
&= f_0(x_2, x_3, x_5, x_6) + g_0(x_5, x_7)\rho_0(x_3) \\
\dot{x}_3 &= \begin{bmatrix} \dot{\phi} & \dot{\theta} \end{bmatrix}^T \\
\dot{x}_4 &= \begin{bmatrix} \ddot{\phi} & \ddot{\theta} \end{bmatrix}^T \\
&= f_1(x_3, x_4, x_6, x_7) + g_1(x_3)\rho_1(x_7) \\
\dot{x}_5 &= \begin{bmatrix} \dot{\psi} & v_z^n \end{bmatrix}^T \\
\dot{x}_6 &= \begin{bmatrix} \ddot{\psi} & \dot{v}_z^n \end{bmatrix}^T \\
&= f_2(x_3, x_4, x_6, x_7) + g_2(x_3)\rho_2(x_7) \\
x_7 &= \begin{bmatrix} \dot{F}_1 & \dot{F}_2 & \dot{F}_3 & \dot{F}_4 \end{bmatrix}^T
\end{aligned} \qquad (18)$$

where

$$f_0 = -\frac{K_t}{m}\begin{bmatrix} v_x^n \\ v_y^n \end{bmatrix}$$

$$g_0 = -\frac{F_1 + F_2 + F_3 + F_4}{m}\begin{bmatrix} s\psi & c\psi \\ -c\psi & s\psi \end{bmatrix} \qquad (19)$$

$$\rho_0 = \begin{bmatrix} s\phi \\ c\phi s\theta \end{bmatrix}$$

$$J_0 = \frac{\partial \rho_0(x_3)}{\partial x_3} = \begin{bmatrix} c\phi & 0 \\ -s\phi s\theta & c\phi c\theta \end{bmatrix}$$

$$f_1 = \begin{bmatrix} \dfrac{1}{I_{xx}} & \dfrac{s\phi t\theta}{I_{yy}} \\ 0 & \dfrac{c\phi}{I_{yy}} \end{bmatrix}\left(\begin{bmatrix} qr(I_{zz} - I_{yy}) \\ pr(I_{xx} - I_{zz}) \end{bmatrix} - K_r\begin{bmatrix} \hat{p} \\ \dot{\hat{\lambda}}_\theta \end{bmatrix}\right)$$

$$\qquad + \begin{bmatrix} t\theta c\phi \\ -s\phi \end{bmatrix}\frac{c(F_1 - F_2 + F_3 - F_4)}{I_{zz}}$$

$$g_1 = \begin{bmatrix} 1 & s\phi t\theta \\ 0 & c\phi \end{bmatrix}\begin{bmatrix} I_{xx} & 0 \\ 0 & I_{yy} \end{bmatrix}^{-1} \qquad (20)$$

$$\rho_1 = \begin{bmatrix} l(F_1 + F_2 - F_3 - F_4) \\ l(F_1 - F_2 - F_3 + F_4) \end{bmatrix}$$

$$J_1 = \frac{\partial \rho_1(x_7)}{\partial x_7} = \begin{bmatrix} l & l & -l & -l \\ l & -l & -l & l \end{bmatrix}$$

$$f_2 = -\frac{K_t}{m}\begin{bmatrix} 0 \\ v_z^n \end{bmatrix} + \begin{bmatrix} 0 \\ g \end{bmatrix}$$

$$\qquad + \begin{bmatrix} \dfrac{c\phi/c\theta}{I_{zz}} & 0 \\ 0 & 0 \end{bmatrix}\left(\begin{bmatrix} \hat{p}\dot{\hat{\lambda}}_\theta(I_{yy} - I_{xx}) \\ 0 \end{bmatrix} - K_r\begin{bmatrix} \dot{\hat{\lambda}}_\psi \\ 0 \end{bmatrix}\right)$$

$$\qquad + \begin{bmatrix} s\phi/c\theta \\ 0 \end{bmatrix}\frac{l(F_1 - F_2 - F_3 + F_4)}{I_{yy}}$$

$$g_2 = \begin{bmatrix} c\phi/c\theta & 0 \\ 0 & -c\phi c\theta \end{bmatrix}\begin{bmatrix} I_{zz} & 0 \\ 0 & m \end{bmatrix}^{-1} \qquad (21)$$

$$\rho_2 = \begin{bmatrix} c(F_1 - F_2 + F_3 - F_4) \\ F_1 + F_2 + F_3 + F_4 \end{bmatrix}$$

$$J_2 = \frac{\partial \rho_2(x_7)}{\partial x_7} = \begin{bmatrix} c & -c & c & -c \\ 1 & 1 & 1 & 1 \end{bmatrix}$$

The final control law can be expressed as :

$$v_1 = A_1 (x_{1d} - x_1) + \dot{x}_{1d}$$

$$v_2 = g_0^{-1} \left[(x_{1d} - x_1) + A_2 (v_1 - x_2) + \dot{v}_1 - f_0 \right]$$

$$v_3 = J_0^{-1} \left[g_0^T (v_1 - x_2) + A_3 (v_2 - \rho_0) + \dot{v}_2 \right]$$

$$v_4 = g_1^{-1} \left[J_0^T (v_2 - \rho_0) + A_4 (v_3 - x_4) + \dot{v}_3 - f_1 \right] \quad (22)$$

$$v_5 = A_5 (x_{5d} - x_5) + \dot{x}_{5d}$$

$$v_6 = g_2^{-1} \left[(x_{5d} - x_5) + A_6 (v_5 - x_6) + \dot{v}_5 - f_2 \right]$$

$$u = \begin{bmatrix} J_1 \\ J_2 \end{bmatrix}^{-1} \left(\begin{bmatrix} g_1 & 0_{2\times2} \\ 0_{2\times2} & g_2 \end{bmatrix}^T \begin{bmatrix} v_3 - x_4 \\ v_5 - x_6 \end{bmatrix} + \begin{bmatrix} \dot{v}_4 \\ \dot{v}_6 \end{bmatrix} + A_7 \begin{bmatrix} v_4 - \rho_1 \\ v_6 - \rho_2 \end{bmatrix} \right)$$

where

$$A_1 = diag([a_1 \quad a_1]), A_2 = diag([a_2 \quad a_2])$$

$$A_3 = diag([a_3 \quad a_3]), A_4 = diag([a_4 \quad a_4])$$

$$A_5 = diag([a_5 \quad a_5]), A_6 = diag([a_6 \quad a_6]) \quad (23)$$

$$A_7 = diag([a_7 \quad a_7 \quad a_7 \quad a_7])$$

The stability of the control structure is analysed by Lyapunov stability theory in (Madani and Benallegue, 2006). If the roll angle and pitch angle are between $\pm \pi / 2$, the whole system is asymptotically stable. In the look angle rate feedback loop, the rate limiter is applied, and the range of rate limiter is ±0.5.

In the next section, the numerical simulation results are presented to verify the IGC.

4 NUMERICAL SIMULATION

For the numerical simulation, a scenario is designed for the indoor precise inspection. A UAV moves toward the inspection panel and keeps the 30 cm distance in the x axis, and tracks the target points in the y and z axes. It is assumed that the eight target points are detected as shown in Figure 7 and the reference trajectory is generated by the target points. The desired target point changes every 7.5 s and a transient function is applied to generate the reference trajectory. The transient function is given as:

$$G(s) = \frac{1}{(s+1)^4} \quad (24)$$

To investigate the nature of the IGC, the target tracking system and the relative navigation filter are

regarded as the ideal models in the numerical simulation. However, for the realistic simulation, the look angle rate is assumed to contain a bias and noise:

$$\hat{\lambda}(k) = \bar{\lambda}(k) + \hat{\lambda}_0 + Q(k)$$

$$\hat{\lambda}_0 \sim U(-0.4 rad / s, \ 0.4 rad / s) \quad (25)$$

$$Q(k) \sim N(0, \ \sqrt{0.1} rad / s)$$

where $\bar{\lambda}(k)$ is an ideal look angle rate of k-th step which is calculated by the geometric equation, $\hat{\lambda}_0$ is a bias term which is generated by the uniform distribution and it is generated in the run-wise, and $Q(k)$ is a Gaussian random noise and it is generated in the path-wise.

Figure 7-Figure 11 show Monte-Carlo simulation results under the errors of the look angle rates, with 150 runs. Note that the Figure 7 depicts the results of all 150 runs of Monte-Carlo simulation and others depict the mean and ±1σ standard deviations. Figure 7 shows the trajectories of the UAV and Figure 8 depicts the tracking errors. Since the waypoint changes before the UAV reaches the target point, the tracking errors are increasing in the middle. However, the tracking errors converges to zero gradually. The additional tracking errors, which are caused by the look angle rate errors, are less than 5 cm and these errors are negligible. Basically, the additional manoeuvring errors occur due to the replacement from the body angular rates to look angle rates. As shown in Figure 8, the additional manoeuvring errors are observed as the biased mean values and the maximum tracking error caused by using the look angle rates is below 2 cm.
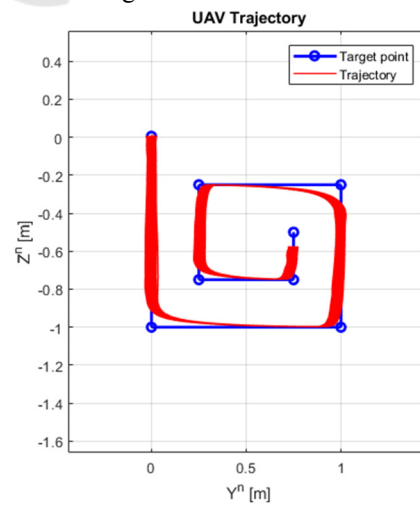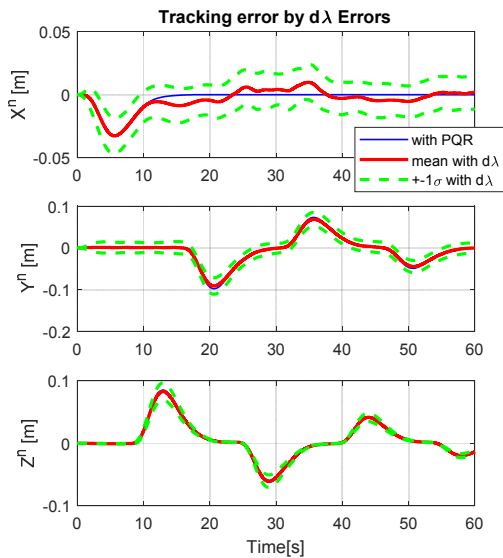

Figure 7: The trajectory of UAV.

Figure 8: The history of the tracking error by $\dot{\lambda}$ errors.

The tracking errors in the x and y axes are larger than the tracking error in the z axis because the body dynamics of the x and y axes is an under-actuated mechanical system. In addition, since the control equation for the x and y axes include the Jacobian matrix about the nonlinear equation, it affects the stability under the noisy condition. As a result, the stability in the x and y axes is relatively more sensitive than the stability along the z axis. However, the tracking errors are below 5 cm during the total flight phase which is reasonable for the indoor inspection.
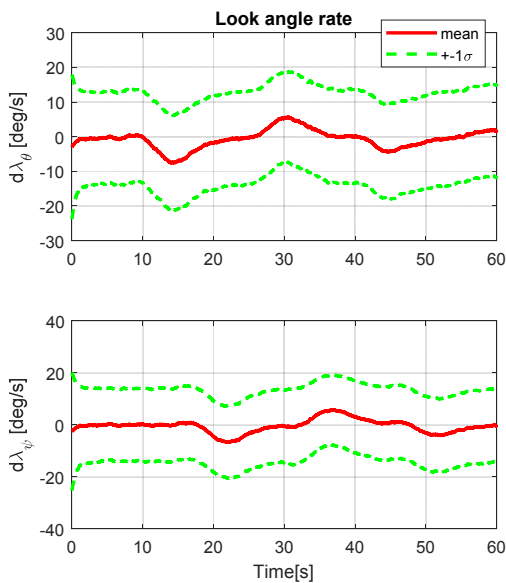
Figure 9-Figure 11 show the time histories of the look angle rates, body angular rates and Euler angles respectively. Before the UAV reaches the desired distance in the x axis, the body attitudes are fluctuating. After the UAV reaches the desired distance in the x axis, attitude in each axis becomes stable. The yaw angles have the bias error as shown in Figure 11 because the look angle rate term in the yaw axis directly influences the yaw angle. However, the figure show that the total amount of tracking errors is tolerable for the indoor inspection. In addition, the proposed IGC keeps the stable state during the total flight phase.
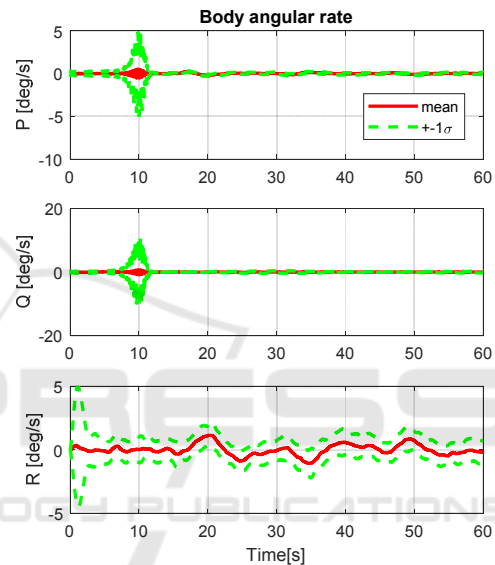

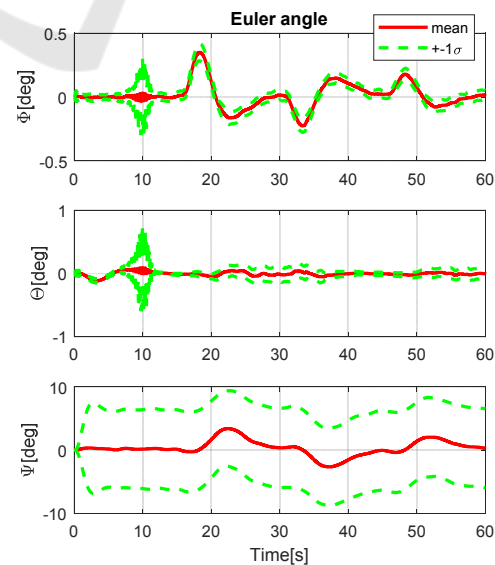Figure 10: The history of the body angular rate.

Figure 9: The history of the look angle rates.

Figure 11: The history of the Euler angles.

5 CONCLUSIONS

This paper proposed an IGNC system for a UAV in the GPS denied environment. The proposed system uses the sensor combination, which consists of an image sensor and a range sensor. As a feasibility study, the performance of the proposed IGC system validated through the numerical simulation. The relative navigation filter and the target tracking system are assumed as the ideal models, but a realistic error model for the look angle rates, which are feedback to the controller, is incorporated in the simulation-based validation.

The proposed IGC has a difference to the conventional attitude controller in terms of the body angular rate loop. The IGC system replaces the body angular rate loop to the look angle rate loop since the look angle rate can be obtained from the image sensor without a gyroscope. Therefore, the gyroscope is not required and we can decrease the number of the sensors required. As a result, the system is subject to the additional manoeuvre, which is caused by the difference between the body angular rate feedback and look angle rates feedback loops, and the look angle rate errors. However, the influence of the additional manoeuvre is small and negligible.

We will extend the back-stepping control structure, incorporating the look angle estimate into the control design, to improve the performance of the integrated system. A practical navigation filter, which is appropriate for the integrated system, will be designed and integrated in the whole system. Also, the proposed IGNC will be verified thorough flight tests.

REFERENCES

Achtelik, M., Bachrach, A., He, R., Prentice, S., Roy, N., 2009. Stereo vision and laser odometry for autonomous helicopters in GPS-denied indoor environments, in: *Unmanned Systems Technology XI.* International Society for Optics and Photonics, p. 733219. https://doi.org/10.1117/12.819082.

Ahrens, S., Levine, D., Andrews, G., How, J. P., 2009. Vision-Based Guidance and Control of a Hovering Vehicle in Unknown, GPS-denied Environments, in: *2009 IEEE International Conference on Robotics and Automation.* IEEE, Kobe,Japan, pp. 2643–2648.

Alarcon, F., Santamaria, D., Viguria, A., 2015. UAV helicopter relative state estimation for autonomous landing on moving platforms in a GPS-denied scenario, in: *IFAC-PapersOnLine.* Elsevier Ltd., pp. 37–42. https://doi.org/10.1016/j.ifacol.2015.08.056.

Blösch, M., Weiss, S., Scaramuzza, D., Siegwart, R., 2010. Vision based MAV navigation in unknown and unstructured environments, in: *Robotics and Automation (ICRA). IEEE international conference,* pp. 21–28. https://doi.org/10.1109/ROBOT.2010.5509920.

Çelik, K., Somani, A.K., 2009. Monocular vision SLAM for indoor aerial vehicles. J. Electr. Comput. Eng. 2013, 1566–1573. https://doi.org/10.1109/IROS.2009.5354050.

Chowdhary, G., Johnson, E.N., Magree, D., Wu, A., Shein, A., 2013. GPS-denied Indoor and Outdoor Monocular Vision Aided Navigation and Control of Unmanned Aircraft. *J. F. Robot.* 30, 415–438. https://doi.org/DOI 10.1002/rob.21454.

Ghadiok, V., Goldin, J., Ren, W., 2011. Autonomous indoor aerial gripping using a quadrotor, in: *IEEE International Conference on Intelligent Robots and Systems.* 2011 IEEE/RSJ International Conference, pp. 4645–4651. https://doi.org/10.1109/IROS.2011.6048786

Kendoul, F., Nonami, K., Fantoni, I., Lozano, R., 2009. An adaptive vision-based autopilot for mini flying machines guidance, navigation and control. *Auton. Robots* 27, 165–188. https://doi.org/10.1007/s10514-009-9135-x.

Madani, T., Benallegue, A., 2006. Backstepping Control for a Quadrotor Helicopter, in: *2006 IEEE/RSJ International Conference on Intelligent Robots and Systems.* IEEE, Beijing, China, pp. 3255–3260. https://doi.org/10.1109/IROS.2006.282433.